

# Further development in the all-sky microwave radiance assimilation and expansion to ATMS in the GSI at NCEP

Yanqiu Zhu<sup>1</sup>, George Gayno<sup>1</sup>, Paul van Delst<sup>1</sup>, Emily Liu<sup>1</sup>, Ruiyu Sun<sup>1</sup>, Joongil Han<sup>1</sup>, John Derber<sup>2</sup>, Fanglin Yang<sup>2</sup>, Jim Purser<sup>1</sup>, Xiujuan Su<sup>1</sup>, Jun Wang<sup>2</sup>, Xu Li<sup>1</sup>

<sup>1</sup>I.M.Systems Group Inc, College Park, MD, <sup>2</sup>NOAA/NCEP/EMC, College Park, MD

## Abstract

Since the implementation of all-sky radiance assimilation of AMSU-A in the operational hybrid 4D Ensemble-Variational (EnVar) Global Forecast System (GFS) at NCEP in 2016, significant progress has been made in the all-sky efforts in the Gridpoint Statistical Interpolation (GSI) analysis system. The all-sky approach has been expanded to radiances of Advanced Technology Microwave Sounder (ATMS), and this makes microwave radiance OmFs among different sensors to be more consistent. Two other efforts on using subgrid-scale clouds and handling of non-Gaussian distribution of radiances are also under investigation for the general enhancement of the all-sky radiance assimilation. Meanwhile, fractional cloud coverage is incorporated in the CRTM 2.3.0.

## 1. Introduction

In the past decade, with the advances of forecast models and the improvement of radiative transfer models, Numerical Weather Prediction (NWP) centers have made steady progress towards utilizing cloudy radiances in addition to radiance observations in clear sky. The European Centre for Medium-Range Weather Forecasts (ECMWF) realized direct all-sky radiance assimilation for the Special Sensor Microwave/Imager (SSM/I) and the Advanced Microwave Scanning Radiometer for Earth Observing System (AMSR-E) in 2009 (Bauer et al. 2010; Geer et al. 2010). Comprehensive studies have also been conducted in other NWP centers such as the Met Office, Japanese Meteorological Agency, Meteo-France, Deutscher Wetterdienst, etc. The capability for all-sky microwave radiance assimilation in the GSI analysis system has been developed at the National Centers for Environmental Prediction (NCEP), and the assimilation of cloudy radiances from the Advanced Microwave Sounding Unit-A (AMSU-A) microwave radiometer for ocean fields of view (FOVs) became operational in the GFS on May 12, 2016 (Zhu et al. 2016) as the GFS was upgraded to the 4D hybrid EnVar system. The assimilation of cloudy AMSU-A radiances in the GFS improves the temperature and relative humidity as well as reducing a known positive bias of stratus.

Since then, significant progress has been made in the all-sky GSI. To facilitate the expansion of the all-sky approach to additional microwave and infrared sensors, the GSI codes for the all-sky capability were generalized, and the all-sky approach has been expanded to ATMS radiances. The all-sky ATMS radiance assimilation is currently being included in the parallel experiment for the upcoming operational implementation in 2018. In the following, this work is presented in section 2. Additional efforts on including subgrid-scale clouds and handling of non-Gaussian

distributions of radiances are also under development for the general enhancement for all-sky radiance assimilation. More discussions are provided in sections 3 and 4 on these two efforts. Meanwhile, the total fractional cloud coverage is incorporated in the CRTM 2.3.0, and its impact on microwave radiances is shown in section 5. Lastly, future work is discussed in section 6.

## 2. Expansion of all-sky radiance assimilation to ATMS

ATMS has 22 channels, combining most of the channels from AMSU-A and Microwave Humidity Sounder (MHS). ATMS is different from AMSU-A and MHS in beam width, number of field of views, and scan swath width. Some channels also have different frequency/polarization.

In this study, since precipitation and snow information from the current operational GFS model are not available for use in the GSI, only radiances affected by non-precipitating clouds and clear-sky radiances are used, and normalized cloud water is used as the cloud control variable. Like all-sky AMSU-A, observation error of ATMS radiance is assigned as a function of the symmetric cloud amount (Geer et al. 2011). The ATMS quality control and bias correction procedures basically follow those of all-sky AMSU-A radiances (Zhu et al. 2016), but ATMS radiances over ice, snow, and mixed surfaces are not used. Efforts have been mainly focused on the special considerations due to unique features of ATMS radiances.

### 2.1 Special quality control considerations in all-sky ATMS radiance assimilation

Unlike AMSU-A, ATMS has varied beam widths, i.e.,  $5.2^\circ$  for channels 1 and 2,  $2.2^\circ$  for channels 3-16, and  $1.1^\circ$  for channels 17-22. In the current operational clear-sky ATMS radiance assimilation, the ATOVS and AVHRR Pre-processing Package (AAPP, NWP SAF/EUMETSAT) spatial averaging is applied to only channels 1-16 to convert the beam widths to  $3.3^\circ$ . In this all-sky ATMS study, the spatial averaging is applied to all channels of ATMS. This facilitates the application of a common beam width of  $3.3^\circ$  for all ATMS channels in calculating FOV and cloud amount/detection.

Moreover, in the operational clear-sky ATMS radiance assimilation, surface properties (including land and sea distribution) at observation locations are calculated as interpolations using the four nearest model surface grid points. This is not appropriate given the T1534/T574 resolution of the GFS 4D EnVar system and the

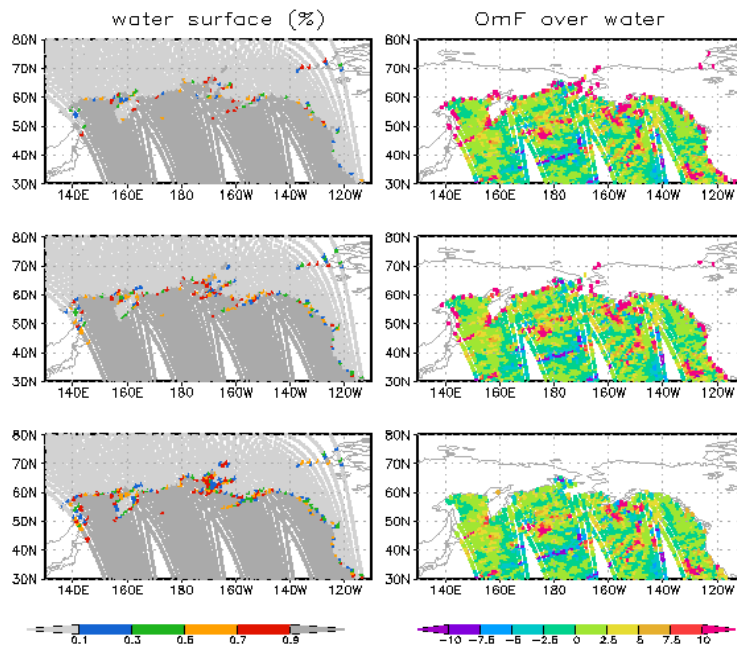


Fig. 1 Water surface percentage (%), left) and OmF (K) over water for ATMS channel 2 (right) with different FOV configurations: interpolation using the four nearest grid points (top), FOV relative antenna power at edge decreasing to 50% (middle) and 1% (bottom) of the maximum at the center.

size of the FOV, and large departures from the first guess (OmF) are observed around coastlines and cryosphere boundaries. The capability of modeling surface properties based on the FOV size and shape is activated for the all-sky ATMS radiances, and the impact of FOV size/shape on the surface property calculation and quality control are investigated, especially for the radiances with large OmFs around coastlines and cryosphere boundaries. The left column of Fig. 1 shows the water surface percentage (%) when surface type is calculated as interpolation using the four nearest model surface grid points (left top) and with FOV calculation where the relative antenna power at the FOV edge decreases to 50% (left middle) and 1% (left bottom) of the maximum at the center. Dark grey color points represent the water surface type locations, and colored points are the mixed surface type locations. As expected, more observation locations are marked as mixed surface type around the coastline when the FOV antenna power at the edge decreases to 1%. Although ATMS radiances with large OmFs are found around the coastline in all three configurations, the quality control procedure of excluding data over mixed surface type makes the difference. The brightness temperature (TB) OmFs of used data over water are displayed in the right column for ATMS channel 2. It is seen that, when interpolation with the nearest 4 model grid points is used for surface property calculations (right top) and when FOV antenna power at edge decreases to 50% (right middle), the observations with large OmFs around the coastline pass the quality control and get used in the GSI. However, these observations are excluded effectively from the system when FOV antenna power at edge decreases to 1% (right bottom).

Additionally, since the precipitation and snow information from the forecast model is not available for use, the radiances affected by strong scattering effects are excluded. The difference of cloud effects on channels 16 and 17 (88.2GHz and 165.5GHz), which are sensitive to ice clouds (right panels of Fig. 2), is calculated as a scattering index (SI) measurement, i.e.,

$$SI = \text{cloud\_effect}(\text{ch16}) - \text{cloud\_effect}(\text{ch17}),$$

where  $\text{cloud\_effect} = TB_{\text{cloudy}} - TB_{\text{clear-sky}}$ .

Figure 2 shows the OmF bias (upper left) and standard deviation (STD, lower left) with respect to observation scattering index for channels 17-22 and cloud effect over ocean for channels 16 (upper right) and 17 (lower right). It is seen that the magnitudes of OmF bias and STD become larger as the scattering index increases. Also, the scattering has the largest impact on channel 17 and smallest impact on channel 22 among these MHS-like channels. Observations from channels 1-7 and 16-22 are excluded if  $(|SI| > 10.0)$  in this study.

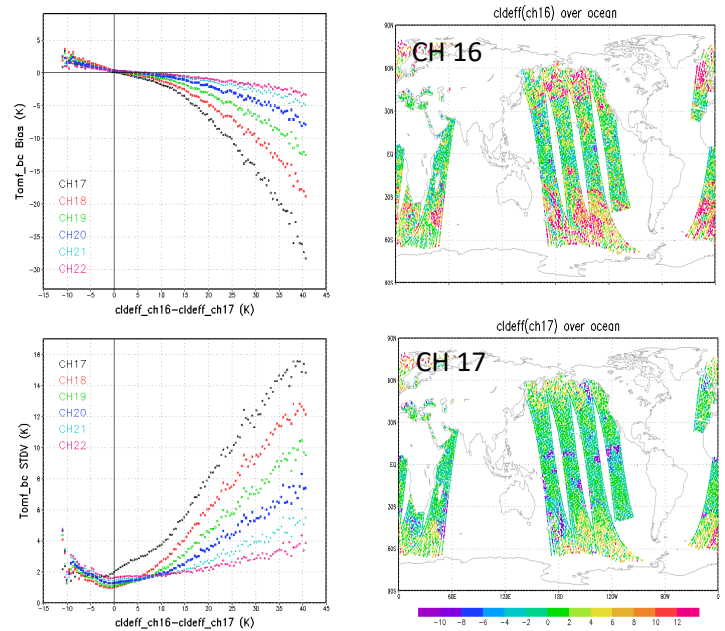


Fig. 2 OmF bias (upper left) and STD (lower left) w.r.t. scattering index, and cloud effect over ocean for channels 16 (upper right) and 17 (lower right).

## 2.2 OmF comparison and data consistency

In a data assimilation system, conflicting observation information will degrade the analysis quality and system performance, hence it is important to assess consistency among different data sources. So far, in the GFS, all-sky AMSU-A radiances are assimilated operationally, but only clear-sky radiances are assimilated for MHS. As ATMS consists of AMSU-A- and MHS-like channels, the radiance OmF statistics are examined for AMSUA, ATMS and MHS in this subsection. The results will help us to gain a better understanding of our usage of observations.

One-month averaged OmF before (left column) and after (right column) bias correction for used radiances of ATMS channel 1 in the clear-sky approach are presented in the top row of Fig. 3, while ATMS and AMSU-A NOAA19 channel 1 in the all-sky approach are shown in the middle and bottom row, respectively. For ATMS radiances in the clear-sky approach, not only clear-sky radiances but also radiances affected by thin clouds are assimilated, and a cloud liquid water bias predictor is applied to remove the cloud effect. When ATMS radiances are assimilated in the all-sky approach, more ATMS radiances affected by clouds are used, and the cloud liquid water bias predictor is removed. It is seen that for ATMS channel 1, although there are significant pattern differences in the OmF before bias correction between the clear-sky and all-sky approach, similar patterns are observed in the OmF after bias correction. This similarity indicates that the cloud liquid water bias predictor in the clear-sky approach works well for channel 1. More importantly, when comparing all-sky ATMS and AMSU-A channel 1, consistent OmF patterns are observed before and after bias correction.

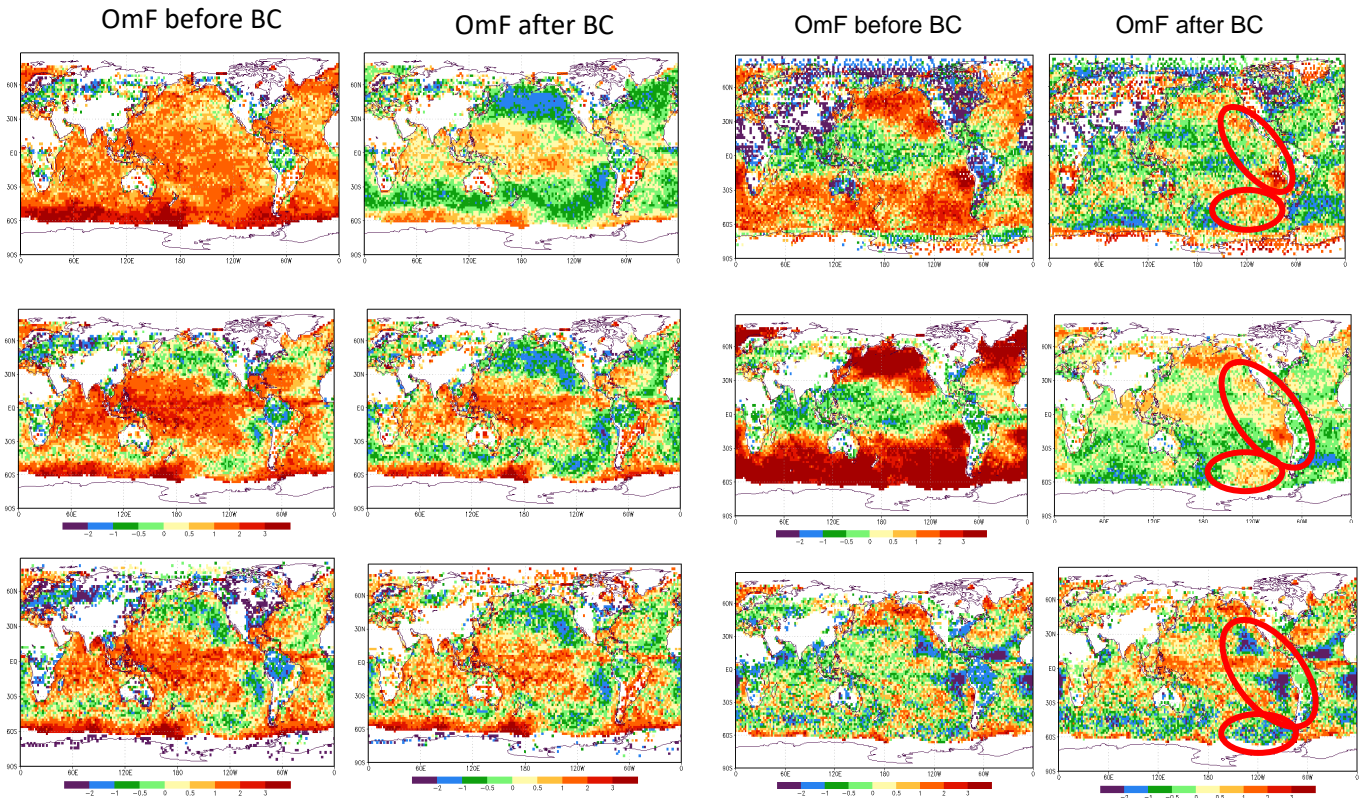


Fig. 3 One-month averaged OmF before (left column) and after (right column) bias correction for ATMS channel 1 in clear-sky approach (top), ATMS (middle) and AMSU-A NOAA19 (bottom) channel 1 in all-sky approach.

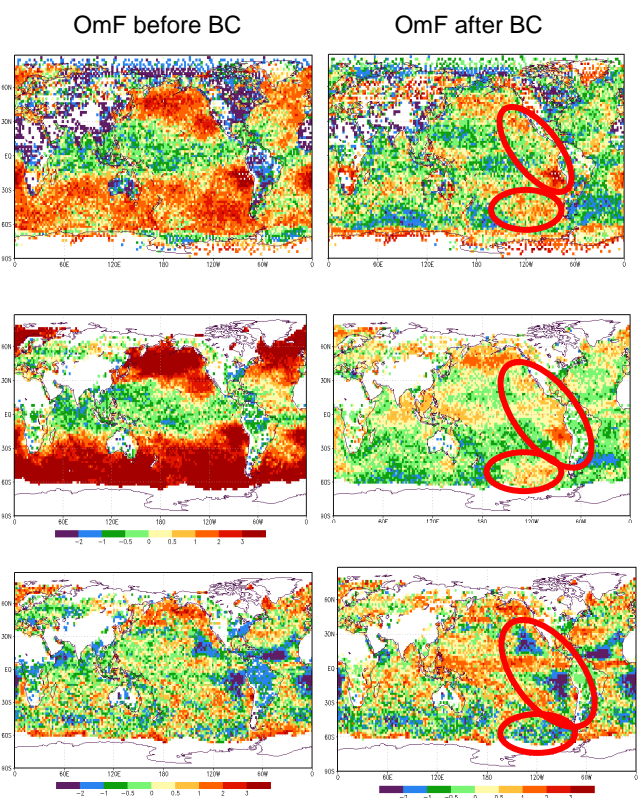


Fig. 4 Same as Fig. 3 but for MHS NOAA18 channel 1 (top), and ATMS channel 16 in clear-sky approach (middle) and all-sky approach (bottom).

However, inconsistencies are noticed between the clear-sky and the all-sky approaches for ATMS channel 16 (Fig. 4). While the OmF patterns for ATMS channel 16 (middle row) and MHS channel 1 (top row) are alike in the clear-sky approach, they are significantly different from the OmF patterns of ATMS channel 16 in the all-sky approach (bottom row) in several regions such as the west of the South American continent. One possible cause for the ATMS channel 16 OmF difference between the clear-sky and all-sky approach may lie in the effectiveness of cloud liquid water bias predictor in the clear-sky approach. Since this bias predictor is calculated using the brightness temperatures of channels 1 and 2 where it seems to be working well (Grody et al., 2009), it may not be adequate for channel 16. The transition from the clear-sky approach to the all-sky approach makes ATMS radiances more consistent among their own low peaking channels and with the all-sky AMSU-A radiances. As for MHS radiances, since only clear-sky radiances are assimilated in the clear-sky approach, the positive bias-corrected OmF west of the South American continent may indicate that some cloudy MHS radiance observations leak through the quality control and are used in the GSI. Stricter quality control may be needed for MHS radiances in the clear-sky approach.

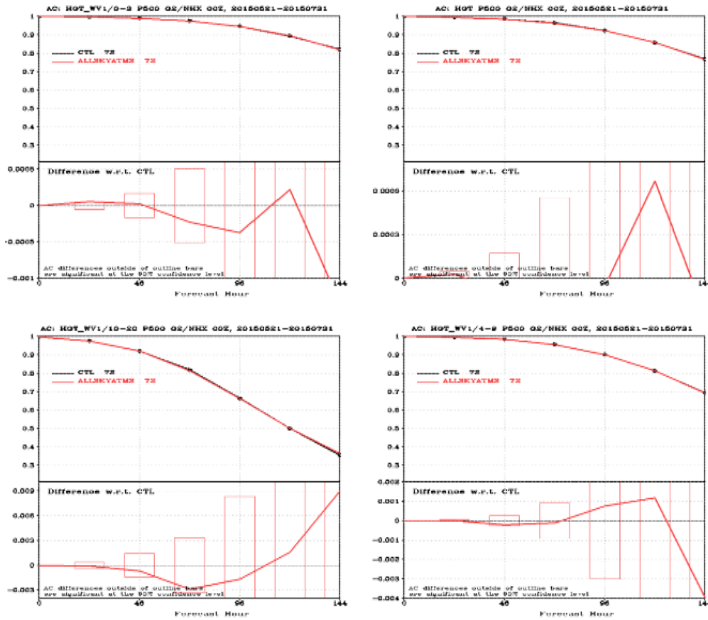


Fig. 5 Anomaly correlation of 500hPa geopotential height (upper part of each panel) in the Northern Hemisphere for wave numbers 10-20 (left lower), 0-3 (left upper), 4-9 (right lower) and all wave numbers (right upper), and the difference with respect to CTL (lower part of each panel).

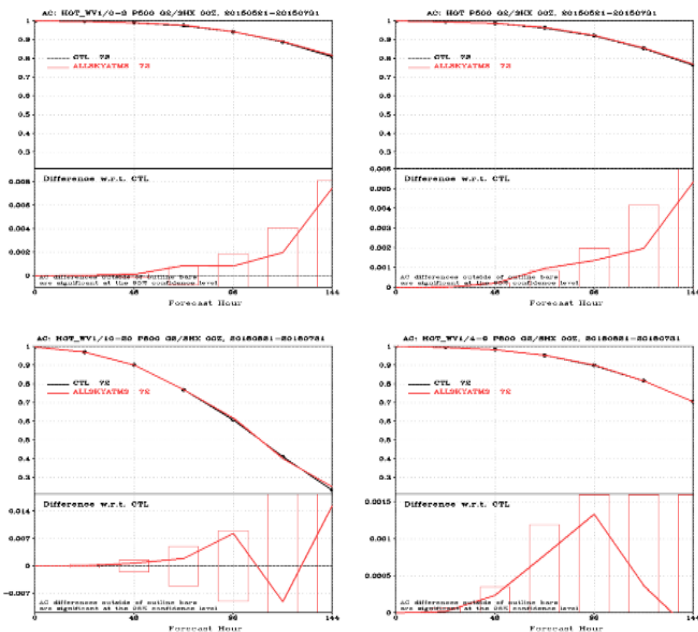


Fig. 6 Same as Fig. 5 but for Southern Hemisphere.

Another clear pattern shown in both all-sky AMSU-A and ATMS OmFs after bias correction (Figures 3 and 4) is the positive OmFs at lower levels in the tropics. In the current GFS forecast model, since rain and subgrid-scale cloud condensate in the convective plume are not available in the forecast model output, only gridscale clouds are used in the radiance simulation calculation for Figures 3 and 4. The lack of model clouds is evident in the

simulated brightness temperature calculation for the lower and middle levels in the tropical ITCZ and SPCZ regions.

### 2.3 Impact on forecast skills

Two-and-a-half month long cycled T670/T254 low resolution data assimilation experiments are performed with the GFS system. The control run, CTL, uses all observations used in the operational GFS system with only AMSU-A radiances being used in the all-sky approach, where ATMS radiances are assimilated in the clear-sky approach. The allskyATMS experiment is different from CTL in that ATMS radiances are assimilated in the all-sky approach. Due to the system spinup, the first week of experimental results are excluded from the statistical calculations used in this study. The assimilation of cloudy ATMS radiances is seen to have a neutral to slightly positive impact on the anomaly correlation of geopotential height at 500 hPa (Fig. 5 for Northern Hemisphere and Fig. 6 for Southern Hemisphere). As for RMS error of wind, mixed results are observed in the Northern Hemisphere and tropics, but improvement is more noticeable in the Southern Hemisphere (Fig. 7).

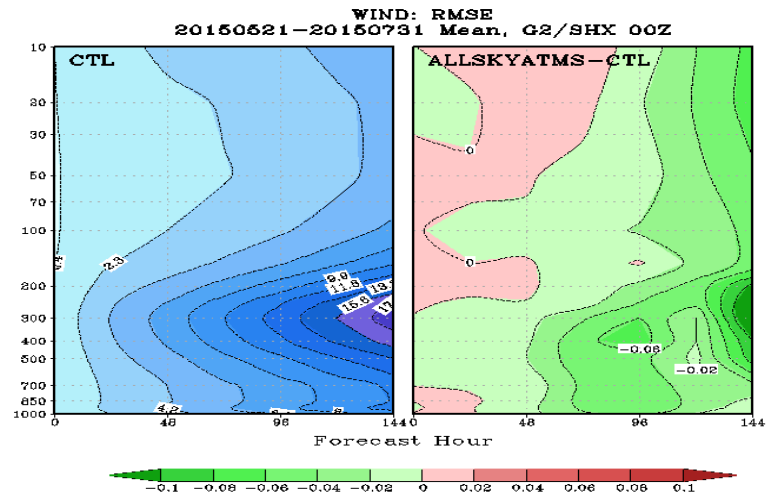


Fig. 7 Wind vector forecast RMSE for the CTL (left) and the RMSE difference between AllskyATMS and CTL (right). Green color represents improvement due to the use of all-sky ATMS radiances.

### 3. Inclusion of convective clouds

As mentioned above, Figures 3 and 4 suggest the lack of model clouds in the TB calculation at the lower and middle levels in the tropics ITCZ and SPCZ regions. In the current operational GFS forecast model, the moist physics schemes consist of the cloud microphysics parameterization (Zhao and Carr 1997, Sundqvist et al. 1989, Moorthi et al. 2001) and parameterizations of deep and shallow cumulus convection (Han and Pan 2011). Snow and precipitation are not written out for the GSI to use. Clouds due to convection are only considered through detraining of the convective cloud water to the grid scale cloud water near the convective cloud tops. Thus the cloud condensate in the

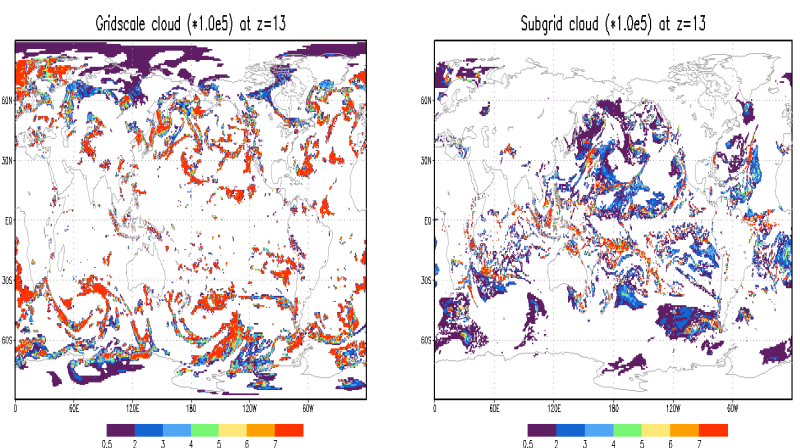


Fig. 8 Gridscale (left) and subgrid-scale (right) cloud water at model level 13 (about 850hPa).

convective plume is also not included in the total condensate of the forecast model output. Hence, only gridscale clouds are available to be used in the simulated radiance calculation for Figures 3 and 4. Figure 8 gives an example of gridscale (left) and subgrid-scale (right)

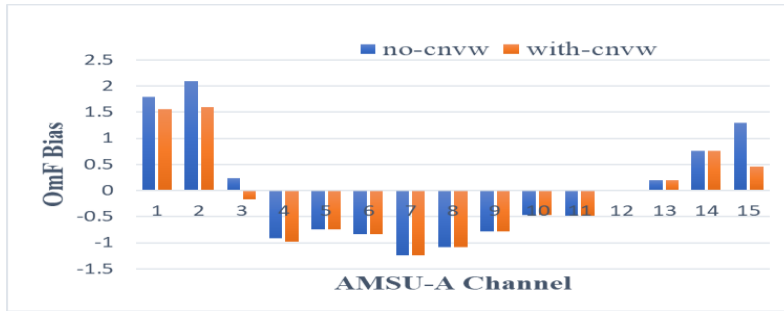


Fig. 9 AMSU-A OmF bias where simulated Tb is calculated with (orange bar) and without (blue bar) subgrid-scale clouds.

convective cloud water at model level 13 (about 850hPa). While the subgrid-scale clouds are included in the forecast model radiation process, these clouds are not available for the GSI. The lack of the subgrid-scale clouds in the GSI will affect not only the simulated radiances but also the ensemble spread of clouds, and subsequently temperature, moisture and cloud analyses, especially at the lower model

levels of the tropics. Hence it is desired to handle these subgrid-scale clouds correctly in the GSI as the radiance observations contain the information of these clouds. The corresponding OmF biases are examined when simulated brightness temperature is calculated with and without subgrid-scale clouds included, and the results are compared in Fig. 9. It is seen that including subgrid-scale clouds (orange bar in Fig. 9) improves OmF biases of AMSU-A channels 1, 2, 3, and 15, and the largest impact is observed in channel 15. The impact of allowing grid- and subgrid-scale clouds to have different optical properties is worthy of exploration in future studies.

It should also be noted that, although the subgrid-scale clouds need to be considered in the radiance data assimilation, these clouds should not be included in the generated cloud analyses nor fed back to the model forecast. Three possible approaches are listed below to include these clouds while preserving the forecast model water budget:

- 1) Combine subgrid and grid scale clouds as one variable in the GSI, but remove subgrid-scale clouds (by employing convective schemes in the GSI) from cloud analyses before passing them back to the model;
- 2) The same as above but do not pass cloud analyses back to the forecast model;
- 3) Treat convective clouds separately as additional control variable(s).

Testing is underway with the current GFS system and, more importantly, will be performed with the new FV3GFS system.

#### 4. Application of new VQC (Purser 2011, 2017) to radiance data

In the GSI, the radiance observation error distribution is assumed to be Gaussian. However, in the all-sky approach, many useful cloudy radiances are associated with large OmFs and exhibit non-Gaussian distributions. Currently, the situation-dependent observation error inflation has been applied to these radiances with large OmFs, so these data can still be used in the analysis with reduced weights while not shocking the system. Since VQC (Andersson and Jarvinen, 1998; Tavalato and Isaksen 2015; etc.) accounts for the non-Gaussian nature of gross measurement errors in its formulation, it is expected that the application of VQC can serve our purpose. The original VQC formulation, a linear combination of Gaussian and flat distributions, has been applied to only conventional data in the GSI. However, this non-Gaussian distribution

may lead to multiple-minima in the cost function. A new probability model for representing realistic measurement errors (Purser 2011), which generalizes the "logistic" distribution, ensures that the negative-log-posterior distribution preserves the property of convexity possessed by the negative-log-prior, and is therefore free of multiple minima. Figure 10 displays the logarithm of normalized OmF histogram (black dots) for AMSU-A NOAA18 during the period from June 1 to July 20, 2015. Green curve represents Gaussian distribution  $f(x)=\exp [-(x-m)^2/(2s^2)]$ , and red curve Logistic distribution  $f(x)=\text{sech}^2 [(x-m)/(2s)]$ . The parameters of the Gaussian and Logistic distributions are estimated using entropy fitting to the OmFs. It is seen that channels 1-5 and 15 resemble logistic distribution while channels 7-10's patterns are quite Gaussian. The generalized logistic distribution  $f(x)=\exp(abx) \text{sech}^{2b} [(x-m)/(\sqrt{2}bs)]$  derived in Purser (2011) can be used for both scenarios with different estimated parameters. As  $b$  increases, the generalized logistic distribution becomes more Gaussian. Preliminary results of the cycling experiments indicate that this new VQC could replace the situation-dependent observation inflation that is currently used on all-sky radiances. As the VQC algorithm is further refined, testing continues with the radiance data.

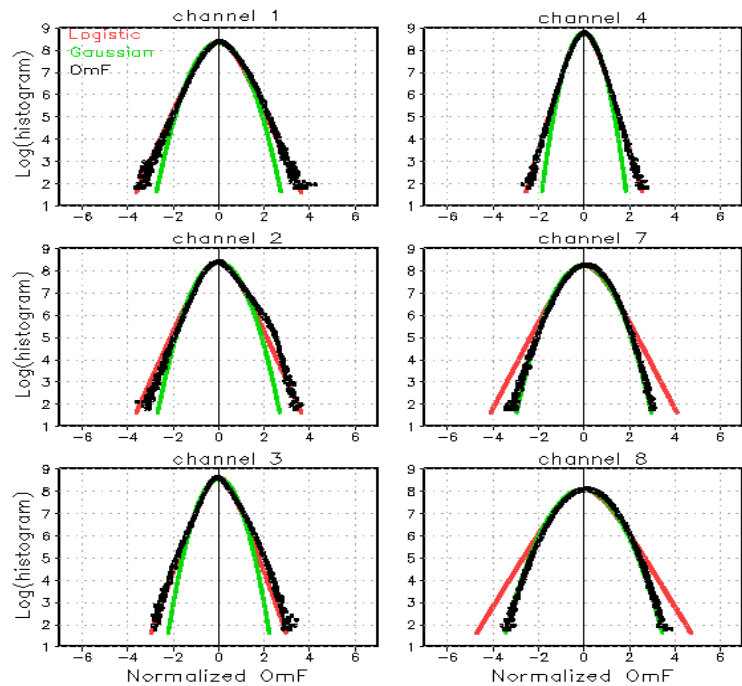


Fig. 10 Logarithm of normalized OmF histogram (black dots) for AMSU-A NOAA18, and curves of Gaussian (green) and Logistic (red) distributions.

## 5. Fractional cloud coverage

In current NCEP operational GFS, the cloud-affected AMSU-A radiances are assimilated under the assumption that the cloudy columns are overcast. In other words, the total cloud cover fraction as viewed by satellite sensor is always one. This is due to two practical reasons that the CRTM does not handle fractional clouds and GFS forecast output does not provide cloud fraction profile to GSI. This is problematic in simulating brightness temperature for the sensor field of view with small-scale variability of cloud and precipitation. At microwave frequencies, the non-linear effect of radiance on hydrometeor amount causes a "beam-filling effect" in satellite observation (Kummerow 1998). Even when two fields of view contain the same mass of hydrometeors, variations in fractional cloud coverage may result in large differences in observed radiances. To better handle the fractional cloudiness conditions, CRTM has enhanced its all-sky capability by implementing various cloud overlap schemes to estimate the total cloud cover and the two-columns radiance calculation to account for partially cloudy scenes (van Delst et al., 2016). The viewing column is split into two parts: clear and cloudy sub-columns. The all-sky brightness temperature which depends on the total cloud cover  $C_{total}$  is

calculated as follows:  $TB_{\text{allsky}} = (1 - C_{\text{total}}) \times TB_{\text{clear-sky}} + C_{\text{total}} \times TB_{\text{cloudy}}$ , where  $TB_{\text{clear-sky}}$  and  $TB_{\text{cloudy}}$  are the brightness temperatures for the clear and cloudy sub-columns, respectively. Three commonly used cloud overlap schemes: maximum, random, and maximum random schemes (Hogan and Illingworth, 2000) had been developed in the CRTM and they are calculated based on the user input of cloud fraction at each model layer. In addition, the hydrometeor weighted cloud cover scheme (averaged scheme) was also implemented following the method proposed

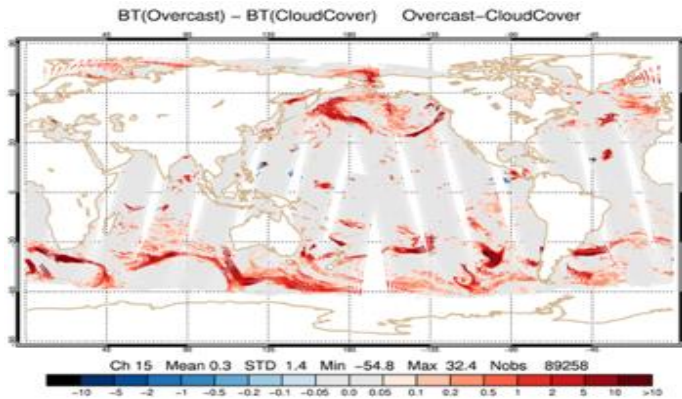


Fig. 11 Impact of cloud fraction on brightness temperature of AMSU-A channel 15.

method, the difference in brightness temperature can be as large as 30 to 50 degrees at rainy and snowy locations. It should be noted that while the averaged scheme is a more appropriate method for estimating the total cloud cover for microwave sensors (since clouds are more transparent to microwave radiation), the maximum-random scheme is probably more appropriate for infrared sensors. The assessment of the impact of cloud fraction on microwave and infrared sensors on analysis and forecast are currently underway. The development in total cloud cover and two-column radiance calculations that handle fractional cloudy scene is incorporated into the CRTM release, Rel-2.3.0.

## 6. Future work and plan

Currently, the forecast models are transitioning to FV3 with more advanced physics at NCEP. So our focus will be on adapting the all-sky radiance assimilation in the FV3 framework, and examining and re-tuning the all-sky radiance assimilation with individual hydrometeors as cloud control variables, should they later become the prognostic variables in the forecast model. As further refinements of all-sky assimilation continue, along with the enhancements of the CRTM, the all-sky radiance assimilation should be expanded to additional instruments and performed for radiances over land.

Moreover, a new effort is in its early development stage to utilize VIIRS cloud products and associated higher level statistics in the all-sky ATMS radiance assimilation. The VIIRS footprints are collocated to the required ATMS footprints. Their cloud products and associated statistics can provide sub-pixel information on the cloudiness needed to optimize the use of all-sky ATMS radiances via both bias correction and quality control procedures.

by Geer and Bauer (2009) for Microwave radiative transfer, in which the total cloud cover is an average cloud fraction over the whole profile, weighted by the total hydrometeor amount. An experimental GFS with precipitation (rain and snow) output was used to investigate the impact of the fractional clouds on simulated brightness temperature. It is found that the impact is small on low frequency

microwave channels, but is larger on high frequency channels. As shown in Fig. 10 for 89 GHz AMSU-A using the averaged

Another aspect that still needs more attention is the choice of the cloud control variable. Although the current cloud control variable works reasonably well, we believe investigation of better cloud control variable in the future will be beneficial, especially when combined with a consideration of the balance among temperature, moisture, and clouds.

#### References:

- Andersson, E. and H. Jarvinen, 1998: Variational quality control. ECMWF Tech. Memo. 250, Reading, UK.
- Bauer, P., A. J. Geer, P. Lopez, D. Salmond, 2010: Direct 4D-Var assimilation of all-sky radiances. Part I: implementation. *Quart. J. Roy. Meteor. Soc.*, **136**, 1868--1885.
- Geer, A. J., P. Bauer, P. Lopez, 2010: Direct 4D-Var assimilation of all-sky radiances. Part II: Assessment. *Quart. J. Roy. Meteor. Soc.*, **136**, 1886--1905.
- Geer, A. J. and P. Bauer, 2009: A revised cloud overlap scheme for fast microwave radiance transfer in rain and cloud. *J. Applied Meteor. Climate.*, **48**, 2257--2270.
- Han, J. and H. L. Pan, 2011: Revision of convection and vertical diffusion schemes in the NCEP Global Forecast System, *Weather and Forecasting*, **26**, 520--533.
- Hogan, R. J. and Illingworth, A. J., 2000: Deriving cloud overlap statistics from radar. *Quart. J. Roy. Meteor. Soc.*, **128**, 2903-2909.
- Kummerow, C., 1998: Beamfilling errors in passive microwave rainfall retrievals. *J. Appl. Meteor.*, **37**, 356-370.
- Moorthi, S., H. L. Pan, P. Caplan, 2001: Changes to the 2001 NCEP operational MRF AVN global analysis/forecast system, NWS Technical Procedures Bulletin 484, available online at <http://www.nws.noaa.gov/om/tpb/484.htm>, 19 pp.
- Purser, R. J., 2011: Mathematical principles of the construction and characterization of a parameterized family of Gaussian mixture distributions suitable to serve as models for the probability distributions of measurement errors in nonlinear quality control, NOAA/NCEP Office Note 468, 42 pp.
- Sundqvist, H., E. Berge, J. E. Kristjansson, 1989: Condensation and cloud parameterization studies with mesoscale numerical weather prediction model, *Mon. Wea. Rev.*, **117**, 1641--1657.
- Tavolato, C. and L. Isaksen, 2015: On the use of a Huber norm for observation quality control in the ECMWF 4D-Var. *Quart. J. Roy. Meteor. Soc.*, **141**, 1514-1527.
- van Delst P., E. H. Liu, L. Bi, 2016: Cloud fraction in the CRTM. JCSDA Office Note CRTM-4, rev71147, 36 pp.
- Zhao, Q. and F. H. Carr, 1997: A prognostic cloud scheme for operational NWP models. *Mon. Weather. Rev.*, **125**, 1931--1953.
- Zhu, Y., J. Derber, A. Collard, D. Dee, R. Treadon, G. Gayno, J. A. Jung, 2014a: Enhanced radiance bias correction in the National Centers for Environmental Prediction's Gridpoint Statistical Interpolation Data Assimilation System, *Quart. J. Roy. Meteor. Soc.*, **140**, 1479--1492.
- Zhu, Y., J. Derber, A. Collard, D. Dee, R. Treadon, G. Gayno, J. Jung, D. Groff, Q. Liu, P. van Delst, E. H. Liu, D. Kleist, 2014b: Variational bias correction in the NCEP's data assimilation system. The 19th International TOVS Study Conference, available online at [http://cimss.ssec.wisc.edu/itwg/itsc/itsc19/program/papers/10\\_02\\_zhu.pdf](http://cimss.ssec.wisc.edu/itwg/itsc/itsc19/program/papers/10_02_zhu.pdf), Jeju Island, South Korea.

Zhu, Y., E. H. Liu, R. Mahajan, C. Thomas, D. Groff, P.v. Delst, A. Collard, D. Kleist, R. Treadon, J. Derber, 2016: All-Sky Microwave Radiance Assimilation in NCEP's GSI Analysis System. *Mon. Weather Rev.*, **144**, 4709--4735.